Particle transport in turbulent flow using both lagrangian and an eulerian formulation

D. Hryb[a,c,*], M. Cardozo[a], S. Ferro[a] and M. Goldschmit[b,c]

[a] *Center for Industrial Research – TenarisSiderca, Dr. Simini 250, B2804MHA, Campana, Argentina*

[b] *Sim&Tec, Av. Pueyrredon 2130, C119ACR, Buenos Aires, Argentina*

[c] *Grupo de Mecánica Aplicada y Tecnología, IMATEC, Engineering School, Universidad de Buenos Aires*

Abstract

Lagrangian and eulerian models for particle transport by a turbulent fluid phase are presented. In both methods, particle distribution results from the action of applied forces (buoyancy, inertial, added mass and drag forces) and turbulent effects are shown. The carrier phase flow –which is solved by finite element method using a k-ε turbulence model– is assumed not to depend on the particles motion. In the lagrangian formulation the dynamic equation for the particles is solved. A discrete random walk model is used to account for the turbulent effects. In the eulerian formulation, the particle concentration is calculated from a convection-diffusion equation using the terminal particles velocity and turbulent diffusivity. Both models are compared to experimental measurements and analytical results; a good agreement is observed.

Nomenclature

C_μ	Constant of k-ε model
C_1	Constant of k-ε model
C_2	Constant of k-ε model
C_D	Drag coefficient
c^p	Dimensionless concentration
C^p	Particle mass concentration
C_c^p	Centerline particle mass concentration
C_o^p	Initila particle mass concentration
D^p	Particle diameter
Dw	Particle-wall distance
g	Gravity acceleration
h	Height
I_o	Modified bessel function of first kind and order 0
J_v	Bessel function of first kind and order v
k	Turbulent kinetic energy
L	Mixing length
m^p	Particle mass
N^p	Number of particles
P	Time averaged pressure
R	Radius
$\mathfrak{Re}^p$	Particle Reynolds number
t	Time
T	Relaxation time
$\mathbf{v}^f$	Time average fluid velocity

v_0^f	Uniform axial fluid velocity
$\mathbf{v}^p$	Particle velocity
v_0^p	Particle velocity initial value
v_T^p	Particle velocity terminal value
$\mathbf{w}$	Normal Gaussian random variable
$\mathbf{x}^p$	Particle position
z_m	Zeros of J_o

Greek simbols

α^p	Particle volume fraction
Δt	Time step
ε	Turbulent kinetic energy dissipation rate
μ^f	Fluid laminar viscosity
η	Dimensionless radial coordinate
ρ^f	Fluid density
ρ^p	Particle density
σ_k	Constant of k-ε model
σ_ε	Constant of k-ε model
σ	Turbulent Schmidt number
θ	Dimensionless time
ξ	Dimensionless position

1. Introduction

Particle transport by a fluid carrier is a phenomenon of great interest since it is frequently found in many scientific fields and industrial processes. Particle dispersion and deposition plays a critical role in several scientific fields and industrial applications:

- inclusion transport in liquid steel [1,2],
- pharmaceutical particle transport and deposition in the human lung [3],
- particle separation in a hydrocyclone [4],
- pollutant transport and deposition in coastal waters [5],
- aerosol transport in flows [6],
- dust pollution in urban area [7],
- dynamic behavior of dross in hot dip bath [8].

The numerical simulation of particle transport by a fluid carrier requires the modeling of the continuous phase (fluid), the discrete phase (particles) and the interaction between them. The continuous phase –whether liquid or gas– is modeled using an Eulerian formulation. The discrete phase –fluid, gaseous or solid– may be approached both from a Eulerian or from a Lagrangian point of view. This has given place to two distinctive strategies, the so called Eulerian-Eulerian and the Eulerian-Lagrangian methods. In the Eulerian-Eulerian approach [4, 6-7, 9-11], particle velocity and concentration fields are calculated for each point of the numerical domain. The Eulerian-Eulerian method can be employed both using a one-fluid formulation [2, 4] and a two-fluid formulation [6-7, 9-11]. In the latter, mass conservation and momentum conservation equations are used to calculate the particle concentration and velocity fields, so the phases are treated as two interpenetrating fluids which interact through their interfacial properties. In the one fluid formulation, on the other hand, no momentum conservation equation is used. Particle velocity is usually determined by an algebraic equation for the particle-fluid slip velocity. In the Eulerian-Lagrangian formulations [5, 12-15], each particle trajectory is simulated. The particle dynamic is generally governed by the Basset-Boussinesq-Oseen (BBO) equation and a random walk model is applied to account for the turbulence effect. In order to solve the BBO equation, the continuous phase properties must be calculated at particle position.

The interaction between phases is modeled according to the strength of the coupling between them. For dense particle concentration, particles action on the fluid and the interaction between particles must be accounted for (four way coupling). For intermediate concentrations, particle interaction can be neglected but particle influence on the continuous phase cannot (two-way coupling). For dilute concentrations, the fluid flow may be considered regardless of the particles flow (one-way coupling). According to Elghobashi [16]), a criterion to determine the type of interaction in terms of the particle volume fraction of particles (α^p) is as follows:

- $\alpha^p < 10^{-6}$, for one-way coupling [1-15].
- $10^{-6} \leq \alpha^p \leq 10^{-3}$, for two-way coupling [17-18].

- $\alpha^p > 10^{-3}$, for four-way coupling [19].

In the present work, we will present both an Eulerian-Eulerian –one fluid– formulation and an Eulerian-Lagrangian formulation and we will use them to solve the same problem. Since both formulations may provide useful information about the particle transport process, our motivation is to show the consistency of both approaches by comparing their results to measurements of particle concentration in free turbulent axisymmetric jet. In the following section the turbulent flow model is presented. In section 3, we describe the Lagrangian and Eulerian formulations. Section 4 contains a series of simple problems used for model verification. In Section 5, the methods are validated by comparison with experimental concentration measurements. Section 6 is devoted to conclusions.

2. Turbulent flow model

The general flow is assumed not to depend on particle dynamics; therefore it is uncoupled from the particle transport model (described in section 3).

The turbulent flow model hypotheses are viscous incompressible flow, isothermal flow, constant fluid density, constant fluid laminar viscosity and a turbulence k-ε model. The following equations are solved:

$$\nabla \cdot \mathbf{v}^f = 0 \tag{1}$$

$$\rho^f \frac{\partial \mathbf{v}^f}{\partial t} + \rho^f \mathbf{v}^f \cdot \nabla \mathbf{v}^f - \nabla \cdot \left[\left(\mu^f + \mu^t \right) \left(\nabla \mathbf{v}^f + \nabla \mathbf{v}^{f T} \right) \right] + \nabla P = \mathbf{0} \tag{2}$$

$$\rho^f \frac{\partial k}{\partial t} + \rho^f \mathbf{v}^f \cdot \nabla k - \nabla \cdot \left[\left(\mu^f + \frac{\mu^t}{\sigma_k} \right) \nabla k \right] - \mu^t \left(\nabla \mathbf{v}^f + \nabla \mathbf{v}^{f T} \right) : \nabla \mathbf{v}^f + \rho^f \frac{C_\mu k^2}{\mu^t / \rho^f} = 0 \tag{3}$$

$$\mu^t = C_\mu \rho^f \sqrt{k} \, L \tag{4}$$

$$\rho^f \frac{\partial \varepsilon}{\partial t} + \rho^f \mathbf{v}^f \cdot \nabla \varepsilon - \nabla \cdot \left[\left(\mu^f + \frac{\mu^t}{\sigma_\varepsilon} \right) \nabla \varepsilon \right] - \rho^f C_\mu C_1 k \left(\nabla \mathbf{v}^f + \nabla \mathbf{v}^{f T} \right) : \nabla \mathbf{v}^f + \rho^f \frac{C_2 \varepsilon^2}{k} = 0 \tag{5}$$

$$L = \frac{k^{3/2}}{\varepsilon} \tag{6}$$

Typical constants of k-ε model of Launder and Spalding [20] are $C_\mu = 0.09$, $C_1 = 1.44$, $C_2 = 1.92$, $\sigma_k = 1.0$ and $\sigma_\varepsilon = 1.0$.

Equations (2-6) are solved implicitly using a standard isoparametric finite element discretization for $\mathbf{v}^f$, k and ε. The incompressibility constrain –Equation (1)– is imposed by penalization [21]. A streamline Upwind Petrov-Galerkin technique [22] is used for stabilization.

The iterative scheme required to solve the equations use the k-L predictor / (ε) corrector algorithm described in [23-24] together with wall functions for boundary conditions [25].

3. Particle transport model.

As mentioned in the introduction, the coupling between the two phases depends on the concentration of particles. We assume that concentration of particles is low enough in order to consider valid the one-way coupling model. This constitutes an important simplification since the fluid and particle dynamics are decoupled and the particle motion is calculated once the fluid flow has been obtained.

The motion of a rigid particle in a viscous flow may be described by an ordinary differential equation derived by Oseen based upon the works of Boussinesq and Basset. When the effect of the previous history of the particle (Basset force term) is neglected, the BBO (Basset-Boussinesq-Oseen) equation may be expressed [26-27].

$$\rho^p \frac{d\mathbf{v}^p}{dt} = \rho^f \frac{d\mathbf{v}^f}{dt} + \left(\rho^p - \rho^f\right)\mathbf{g} + \frac{3}{4}\frac{\rho^f}{D^p}C_D\left(\mathbf{v}^f - \mathbf{v}^p\right)\left|\mathbf{v}^f - \mathbf{v}^p\right| - \frac{\rho^f}{2}\frac{d\left(\mathbf{v}^p - \mathbf{v}^f\right)}{dt} \quad (7)$$

Equation (7) represents the Newton law for a spherical particle of density ρ^p, diameter D^p and velocity $\mathbf{v}^p$. Terms on the right hand side are volume forces acting on the particle. Four different forces are taken into account in Equation (7):

▪ the inertial force (first term on the right hand side) which depends on local fluid velocity $\mathbf{v}^f$ and fluid density ρ^f,

▪ the buoyancy force (second term on the right hand side) due to the action of gravity acceleration,

▪ the drag force (third term on the right hand side), characterized by the coefficient C_D –to be discussed below– and

▪ the added mass force (last term on the right hand side) that takes into account the fact that the fluid near the particle is also being accelerated.

The drag coefficient C_D is found to depend only on the particle Reynolds number, $\Re e^p = \rho^f D^p \left|\mathbf{v}^f - \mathbf{v}^p\right| / \mu^f$. The function $C_D\left(\Re e^p\right)$ was obtained experimentally and may be approximated by [28],

$$C_D = \frac{24}{\Re e^p} \qquad\qquad \Re e^p < 0.1$$

$$C_D = \left(\frac{24}{\Re e^p}\right)\left(1 + 0.14\,\Re e^{p\,0.7}\right) \qquad 0.1 < \Re e^p < 1000 \qquad\qquad (8)$$

$$C_D = 0.445 \qquad\qquad 1000 < \Re e^p < 350000$$

3.1 Lagrangian formulation.

In a Lagrangian formulation of the particle transport process, the motion of particles is described by solving a set of ordinary differential equations along the trajectory in order to calculate the change of particle location and the components of particle velocity.

Particle velocity is calculated from the contributions of a term resulting from the solution of the BBO equation, $\mathbf{v}^p$, and a second term that takes into account turbulent fluctuations of the flow field. The BBO equation is solved for each particle using a backward Euler scheme. Particle velocity due to turbulent fluctuations is obtained using a discrete random walk model. As a result of these, two particles with same initial conditions may have different trajectories. When many particles are considered, an effective diffusion results from turbulence effects.

Taking into account the mean velocity and the turbulent velocity, particle position is updated according to

$$\mathbf{x}^p(t+\Delta t) = \mathbf{x}^p(t) + \frac{\mathbf{v}^p(t+\Delta t) + \mathbf{v}^p(t)}{2}\Delta t + \nabla\left(\frac{\mu^t}{\sigma\,\rho^f}\right)\Delta t + \sqrt{2\,\frac{\mu^t}{\sigma\,\rho^f}}\,\mathbf{w}(t+\Delta t) \qquad (9)$$

where $\mathbf{w}$ is a random variable with a normal gaussian distribution with a zero mean and a Δt variance [29]. σ is the turbulent Schmidt number, assumed constant throughout this paper. Turbulence viscosity is given by the k-ε model discussed in the previous section.

In order to calculate the particle velocity, flow variables are required at current particle position. Thus, it is necessary to know which element the particle is in. All the elements are inspected beginning with the one where the particle was in the previous time step and going on with first neighbors (see Figure 1a). For a given element, if the particle coordinates are within the maximum and minimum element coordinates (black dashed rectangle, see Figure 1b) particle natural coordinates (r,s) are calculated. The particle is inside the element if its natural coordinates are within the [-1 1] interval.

Particle-wall collisions become of importance in confined flows. We consider a hard sphere model for wall collision that implies a negligible particle deformation during the impact process. Once a particle displacement modulus Δx is obtained, all nodes with particle-wall distances $Dw < \Delta x$ are selected (see Figure 2). For every wall element, intersection between $\Delta\underline{x}$ segment and the boundary segments is looked for. The final position of the particle is obtained by reflecting the particle on the solid wall. Wall rugosity may be taken into account by a random perturbation on the reflection angle.

3.2 Eulerian formulation.

In an Eulerian formulation of the mass transport process, particle trajectories are not calculated. The mass concentration of particles, C^p , as function of time and space is calculated instead,

$$C^p(\mathbf{x},t) = m^p\,Lim_{\Delta V \to 0}\,\frac{N^p}{\Delta V} \qquad (10)$$

where $N^p(\Delta V)$ is the number of particles present in volume ΔV located at $\mathbf{x}$ and m^p is the particle mass. In the present analysis, all particles are assumed to have the same density and size.

The particle mass conservation requires that C^p satisfies the following relation,

$$\frac{\partial C^p}{\partial t} + \nabla \cdot \mathbf{F}(\mathbf{x},t) = 0 \tag{11}$$

where $\mathbf{F}(\mathbf{x},t)$ is the particle mass flow, which has contributions from both the average flow and from turbulent fluctuations, $\mathbf{F} = \mathbf{v}^p\, C^p + \mathbf{F}_{turb}$. The mean velocity is obtained from the BBO equation. Since turbulent fluctuations are unknown, their contribution to the particle mass flow requires to be model. Assuming a linear relation between the turbulent component of $\mathbf{F}$ and the concentration gradient, the following expression is obtained

$$\mathbf{F}(\mathbf{x},t) = \mathbf{v}^p(\mathbf{x},t)\, C^p(\mathbf{x},t) - \frac{\mu^t(\mathbf{x},t)}{\rho^f \sigma}\, \nabla C^p(\mathbf{x},t) \tag{12}$$

Using the above expression for the particle mass flow on the conservation equation, a partial differential equation for $C^p(\mathbf{x},t)$ is found,

$$\frac{\partial C^p}{\partial t} + \mathbf{v}^p \cdot \nabla C^p + C^p\, \nabla \cdot \mathbf{v}^p = \nabla \cdot \left(\frac{\mu^t}{\rho^f \sigma} \nabla C^p \right) \tag{13}$$

Since particle dynamics were assumed not to have influence on the fluid flow, velocity and turbulent viscosity fields do not depend on the concentration and the problem results linear.

Equation (13) is a transport-diffusion equation and was solved using isoparametric finite elements with Streamline Upwind Petrov Galerkin stabilization technique [22]. Special attention must be paid to the term $C^p\, \nabla \cdot \mathbf{v}^p$ that takes into account the fact that the particle velocity field is not necessarily solenoidal.

In order to solve Equation (13), proper boundary and initial condition should be specified for the equation to have a unique well posed solution. The problem requires initial values of C^p in the whole numerical domain and prescribed C^p values or its normal derivative in the boundaries.

The particle velocity field, $\mathbf{v}^p$, is obtained from the BBO equation, neglecting the particle acceleration with respect to the fluid acceleration,

$$\left(\rho^f - \rho^p \right) \left(\mathbf{g} - \frac{d\mathbf{v}^f}{dt} \right) = \frac{3}{4} \frac{\rho^f}{D^p} C_D \left(\mathbf{v}^f - \mathbf{v}^p \right) \left| \mathbf{v}^f - \mathbf{v}^p \right| \tag{14}$$

For a small particle Reynolds number, $C_D \left| \mathbf{v}^f - \mathbf{v}^p \right| = 24\mu^f / \left(\rho^f D^p \right)$ and the following expression is found for the particle velocity,

$$\mathbf{v}^p = \mathbf{v}^f + \tau \left(\mathbf{g} - \frac{d\mathbf{v}^f}{dt} \right) \qquad ; \qquad \tau = \frac{\left(\rho^p - \rho^f \right) D^{p2}}{18\mu^f} \tag{15}$$

The above expression has been successfully used in the flow calculation of a hydrocyclone where centrifugal forces are relevant [see, for instance, 30 and 31].

4. Verifications.

In order to verify the models described in the previous section, different test cases with simplified geometry and physics were analyzed. Numerical results were compared to available analytical solutions. Sub-sections 4.1 and 4.2 are devoted to the Lagrangian and Eulerian models respectively. In Sub-section 4.3 we present a test case where both models may be verified simultaneously.

4.1 Lagrangian model verification.

The Lagrangian model was verified by analyzing the velocity and the trajectory of a wooden sphere in water. The sphere starts moving along the gravity direction, then slows down and reverses its direction to finally reach the terminal velocity. The following solution holds for particle velocity and position

$$
\begin{aligned}
v^p = v_T^p \tan(\theta_0 - \theta) \qquad & x^p = \frac{v_T^p T}{2} \ln(2\cos(2\theta - 2\theta_0) + 2) - x_1 \qquad & if \quad \theta < \theta_0 \\
v^p = v_T^p \tanh(\theta_0 - \theta) \qquad & x^p = v_T^p T\left(\theta - \ln(e^{2\theta_0} + e^{2\theta})\right) - x_2 \qquad & if \quad \theta > \theta_0
\end{aligned}
\tag{19}
$$

where $\theta_0 = \tan^{-1}(v_0^p / v_T^p)$, $x_1 = v_T^p T \ln(2\cos(2\theta_0) + 2)/2$, $x_2 = -v_T^p T(\theta_0 - \ln(4)) + x_1$.

Our Lagrangian numerical results and analytical solutions are compared in Figure 3.

4.2 Eulerian model verification.

Verifications for the Eulerian model were carried out by analyzing the flow on a cylinder (height h and radius R) with uniform initial concentration C_0^p and uniform turbulent viscosity μ^t. Numerical results for the dimensionless concentration $c^p = C^p / C_0^p$ were compared to analytical solutions for three different test cases. An small particle Reynolds number was assumed.

Case 1: Uniform flow

We first considered the time and spatial evolution of the concentration when the fluid flows with uniform axial velocity v_0^f. The concentration only depends on the axial coordinate, so the problem requires boundary conditions at $z=0$ and $z=h$ to be specified.

The following analytical solution holds when homogenous Dirichlet boundary conditions are applied,

$$
c^p = \sum_{m=1}^{\infty} \frac{1 - e^{-\frac{1}{2}\lambda}(-1)^m}{1 + 4k_m^2} \frac{8k_m}{\lambda} \exp\left(-\left(k_m^2 + \frac{1}{4}\right)\theta\right) \exp\left(\frac{\zeta}{2}\right) \sin(k_m \zeta)
\tag{20}
$$

with $\theta = \dfrac{\rho^f (v_0^f + \tau g)^2}{\mu^t} t$, $\zeta = \dfrac{\rho^f (v_0^f - \tau g)}{\mu^t} z$, $\lambda = \dfrac{\rho^f (v_0^f - \tau g)}{\mu^t} h$ and $k_m = \dfrac{\pi n}{\lambda}$.

Comparison of our Eulerian numerical results and analytical solutions for $\lambda = 7.5$ are presented in Figure 4.

Case 2: Fluid at rest

As a second example we considered flow at rest and analyzed the evolution of concentration due to diffusion through the cylinder lateral surface (with a homogenous Dirichlet boundary condition). The problem depends only on the radial coordinate. The corresponding analytical solution is

$$c^p = \sum_{m=1}^{\infty} A_m \exp\left(-z_m^2 \theta\right) J_0\left(z_m \xi\right) \tag{21}$$

where $\theta = \left(R^2 \mu^t / \rho^f\right)t$, $\xi = r / R$ and $A_m = 2\left(z_m J_1(z_m)\right)^{-2} \int_0^{z_m} J_0(\eta)d\eta$.

A comparison of our Eulerian numerical and analytical results is shown in Figure 5.

4.3 Joint Lagrangian and Eulerian verification

As a final verification of the model, we considered the axisymmetric diffusion of particles trough a homogenous fluid at rest in an unbounded domain. The problem is defined by the particles initial distribution and their diffusivity in the fluid, κ^p. For an initial concentration given by,

$$C^p = \begin{cases} C_0^p & \text{if } r < R \\ 0 & \text{if } r > R \end{cases} \tag{23}$$

the analytical solution is

$$c^p = \frac{1}{\theta}\exp\left(\frac{-\xi^2}{2\theta}\right) \int_0^1 \exp\left(\frac{-\eta^2}{2\theta}\right) I_0\left(\frac{\xi\eta}{\theta}\right)\eta\, d\eta \tag{24}$$

where $c^p = C^p / C_0^p$, $\xi = r / R$ and $\theta = 2\kappa^p t R^{-2}$. I_0 is the modified Bessel function of the first kind and order 0.

This problem may be approached by both the Lagrangian and Eulerian formulations. The corresponding results are shown in Figure 6.

5 Validation

In order to validate both the Lagrangian and Eulerian model, we analyzed the flow and concentration field due to an isothermal, turbulent, axisymmetric air free jet. Numerical results are compared to experiments carried out by Becker et al [32].

The jet is discharged into stagnant room air, with negligible temperature variation, from essentially an ideal flow nozzle of *0.635 cm* throat diameter and *2.41cm* upstream tube diameter. The nozzle air was

marked with an oil smoke. The nozzle air velocity is of *130 m/s*, giving a nozzle Reynolds number of *54000* (see Figure 7).

The concentration radial profile is found to become self-preserving about 40 nozzle radii downstream of the nozzle. Results are expressed in terms of the normalized concentration C^P/C^P_c as function of the dimensionless radial coordinate $\eta=r/(d-4.8r_0)$, where C^P_c is the centerline concentration $C^P_c = C^P(r=0)$, r_0 is the nozzle radius and d is the axial position.

Both the Lagrangian and Eulerian formulations may be applied to model this problem. The corresponding results will be compared to experimental data reported in [32]. A turbulent Schmidt number of 0.78 was found to provide the best fitting with experiments, which is consistent with results presented in reference [33]. Both methods proved to be adequate to simulate the particle concentration distribution in this kind of problems.

Fluid dynamics and Eulerian formulation results were obtained on a 24,000 nodes mesh. The Lagrangian formulation results were obtained by analyzing trajectories of 80,000 particles. In order to compare results, the Lagrangian method requires the particles concentration at the sample point to be calculated. For any given time step, the number of particles N^p in a volume V centered at the sample point is counted and the concentration is estimated by $C^p = N^p/V$. The volume V is chosen large enough to include a representative number of particles and small enough to keep the calculation as local as possible.

Comparison between the Eulerian and Lagrangian formulatins are presented in Figure 8. The Figure presents a general qualitative agreement between both formulations in the whole domain.

For a quantitative comparison Figure 9 and 10 present data from both formulations together with experimental results, showing remarkable agreement.

6. Conclusions

Lagrangian and Eulerian formulations have been developed to model particle transport in a turbulent flow. Both formulations were verified in test cases and used to simulate the particles concentration generated by an isothermal, turbulent, axisymmetric free jet. Results showed good agreement with the experiment and pointed out the consistency of both formulations.

Compared to the Eulerian approach, the Lagrangian formulation provides a better insight of particle dynamics, enabling an easy treatment of particle transients, particle collisions and coalescence and wall collisions. On the other hand, the Lagrangian formulation becomes computationally expensive when a large number of particles is involved and usually requires post processing of results.

For this reason, Lagrangian and Eulerian formulations are complementary and, in many industrial applications, both approaches become relevant. However, the consistency of both approaches must be accounted for. It is important to note that, in the present numerical calculations, the concentration distribution as predicted by the Lagrangian formulation *do tend* to that predicted by the Eulerian formulation, provided the number of particles is large enough. This consistency is achieved by using a discrete random walk model that correctly represents the turbulent effects on the particle trajectory.

References

[1] B.G. Thomas, L. Zhang, Mathematical modeling of fluid flow in continuous casting, ISIJ International 41 (2001) 1181-1193.

[2] A.K. Sinha, Y. Sahai, Mathematical modeling of inclusion transport and removal in continuous casting tundishes, ISIJ internationa 33 (1993) 556-566.

[3] R.F. Kunz, D.C. Haworth, L.S. Leemhuis, A.C. Davison, S. Zidowitz, A. Kriete, Eulerian multiphase CFD analysis of particle transport and deposition in human lung, Proceedings of Biomedicine 2003, Ljubljana, Slovenia, 2003.

[4] M.R. Davison, Numerical calculations of flow in a hydrocyclone operating without an air core, Appl. Math. Modelling, 12 (1988) 120-128.

[5] D. Spivakovskaya, A.W. Heemink, G.M. Milstein, J.G.M. Schoenmakers, Simulation of the transport of particles in coastal waters using forward and reverse time diffusion, Advances in Water Resources 28 (2005) 927-938.

[6] P. Armand, D. Boulaud, Two fluid modeling of aerosol transport in laminar and turbulent flows, J. Aerosol Sci 29 (8) (1998) 961-983.

[7] S. Laslandes, C. Sacre, Transport of particles by a turbulent flow around an obstacle – a numerical an a wind tunnel approach, J. Wind Engineering and Industrial Aerodynamics 74-76 (1998) 577-587.

[8] J. Kurobe, M. Iguchi, Cold model experiment on dynamic behavior of dross in hot dip plating bath, Science and technology of advanced materials 1 (2000) 251-259.

[9] A. Kaufmann, O. Simonin, T. Poinsot, Direct numerical simulation of particle-laden homogeneous isotropic turbulent flows using a two fluid model formulation, Proceedings of the 5th International conference of multiphase flow, ICMF 2004; pp. 443.

[10] A. Mitter, J.P. Malhorta, H.T. Jadeja, The two-fluid modeling of gas particle transport phenomenon in confined system considering inter particle collision effects, International Journal of Numerical Methods for heat and fluid flow 14 (5) (2004) 579-605.

[11] M. Sommerfeld, Analysis of collision effects for turbulent gas–particle flow in horizontal channel: Part I. Particle transport, International Journal of Multiphase Flow29 (2003) 675–699.

[12] C.F.M. Coimbra, J.S. Shirolkar, M. Queiroz McQuay, Modeling particle dispersion in a turbulent multiphase mixing layer, Journal of Wind Engineering and Industrial Aerodynamics 73 (1998) 79-97.

[13] G. Willgoose, A hydrodynamic particle tracking algorithm for simulating settling of sediment, Mathematics and Computers in Simulation 43 (3-6) (1997) 343-349.

[14] Y. Xiong, M. Zhang, Z. Yuan, Three-dimensional numerical simulation method for gas–solid injector, Powder Technology 160 (3) (2005) 180-189.

[15] X. Yang, N.H. Thomas, L.J. Guo, Particle dispersion in organized vortex structures within turbulent free shear flows, Chemical Engineering Science 55 (7) (2000) 1305-1324.

[16] S. Elghobashi, On predicting particle-laden turbulent flows, Applied Scientific Research 52 (1994) 309-329.

[17] A. Ferrante, S. Elghobashi, On the physical mechanisms of two-way coupling in particle-laden

isotropic turbulence, Physics of fluids 15 (2) (2003) 315-329.

[18] S. Elghobashi, G.C. Truesdell, On the two-way interaction between homogeneous turbulence and dispersed solid particles I: Turbulence modification, Physics of Fluids A 5 (7) (1993) 1790-1801.

[19] A. Smirnov, I. Celik, A lagrangian particle dynamics model with an implicit four-way coupling scheme, Proceedings of the International Mechanical Engineering Congress & Exposition Orlando, Florida, USA, 2000.

[20] B.E. Launder, D.B. Spalding, The numerical computation of turbulent flows, Comp. Meth. in Appl. Mech. And Eng. 3 (1974) 269-289.

[21] A.N. Brooks, T.J.R. Hughes, Streamline upwind Petrov-Galerkin formulations for convection dominated flows with particular emphasis on the incompressible Navier-Stokes equation, Comp. Meth. Appl. Mech. Eng. 32 (1982) 199-259.

[22] O.C. Zienkiewicz, L.R. Taylor, In The Finite Element Method, 5th. Edition, Mc Graw Hill, London, 2000.

[23] M.B. Goldschmit, M.A. Cavaliere, Modelling of turbulent recirculating flows via an iterative (k-L)-predictor / (ε)-corrector scheme, Applied Mechanics Review 48 (11) (1995) 211-215.

[24] M.B. Goldschmit, M.A. Cavaliere, An iterative (k-L)-predictor / (ε)-corrector algorithm for solving (k-ε) turbulent models, Engineering Computations 14 (4) (1997) 441-455.

[25] R.J. Príncipe, M.B. Goldschmit, Las condiciones de contorno sobre la pared en el modelado de flujo turbulento, Proceedings of the VI Congreso Argentino de Mecánica Computacional MECOM'99, Mendoza, Argentina, 1999.

[26] C.F.M. Coimbra, R.H. Rangel, General solution of the particle momentum equation in unsteady Stokes flow, Journal of Fluid Mechanics 370 (1998) 53-72.

[27] M.R. Maxey, J.J. Riley, Equation of motion for a small rigid sphere in a nonuniform flow, Physics of Fluids 26 (4) (1983) 883-889.

[28] R.H. Perry, D.W. Green, Perry's Chemical Engineers' Handbook, McGraw Hill.

[29] Bernt Oksendal, Stochastic Diferential Equations: An Introduction with Applications, 5th Edition, Springer-Verlag.

[30] K.A. Pericleous; N. Rhodes, The hydrocyclone classifier – a numerical approach, International Journal of Miner. Process 17 (1986) 23-43.

[31] M.R. Davidson, Numerical calculation of flow in a hydrocyclone operating without an air core, Applied Mathematical Modelling 12 (2) (1988) 119-128.

[32] H.A. Becker, H.C. Hottel, G.C. Williams, The nozzle-fluid concentration field of the round turbulent free jet, Journal of Fluid Mechanics 30 (1967) 285-303.

[33] I. Yimer, I. Campbell, L.Y. Jiang, Estimation of the turbulent Schmidt number from experimental profiles of axial velocity and concentration for high-Reynolds-number jet flows, Canadian Aeronautics and Space Journal 48 (3) (2002) 195-200.
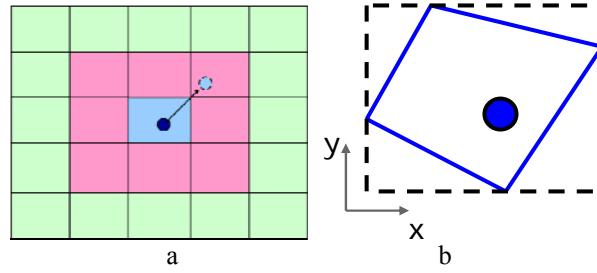
Figures
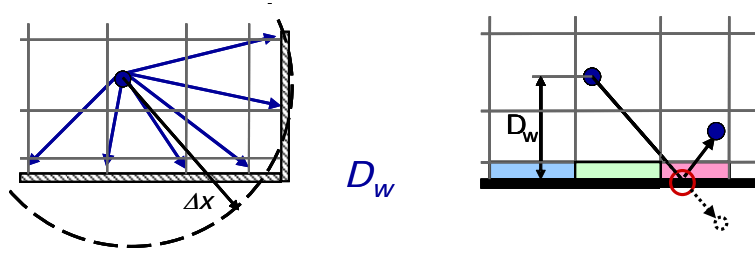

Figure 1: particle localization

D_W

Figure 2: particle-wall collision
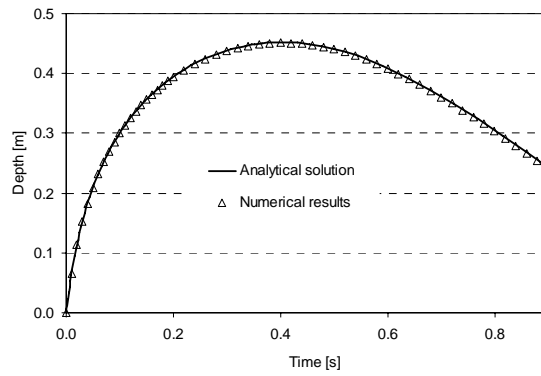

Figure 3: Time evolution of a wood particle in water. Comparison of numerical and analytical solutions for $v_0^p = 8\,m/s$, $D^p = 0.05m$, $\rho^p = 700 Kg/m^3$ and $\rho^f = 1000 Kg/m^3$
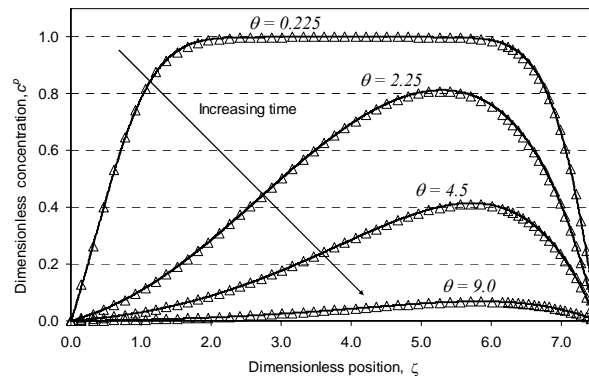

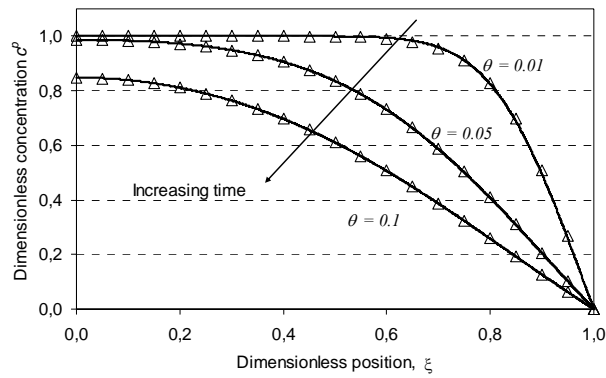Figure 4: Comparison of numerical solution (triangles) and analytical results (lines) for different time steps.

Figure 5: Comparison of numerical solution (triangles) and analytical results (lines) for different time steps.
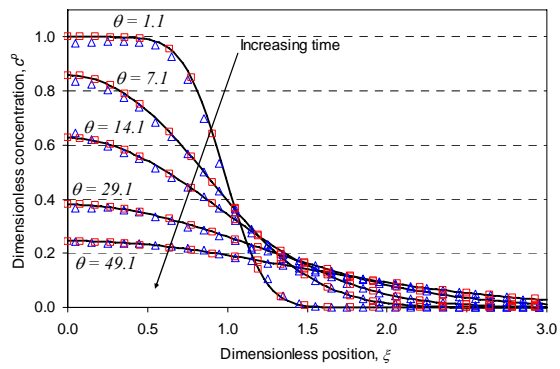
Figure 6: Analytical solution (black lines), Eulerian model results (red squares) and Lagrangian model results (blue triangles) for axisymmetric diffusion problem.
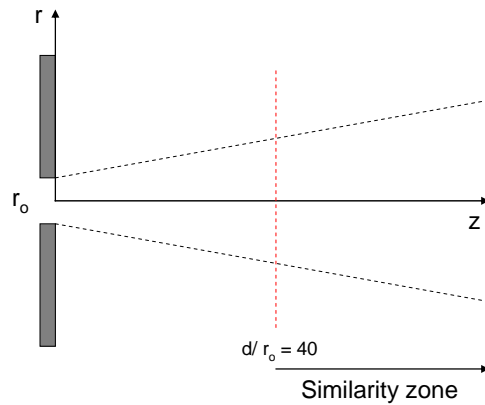

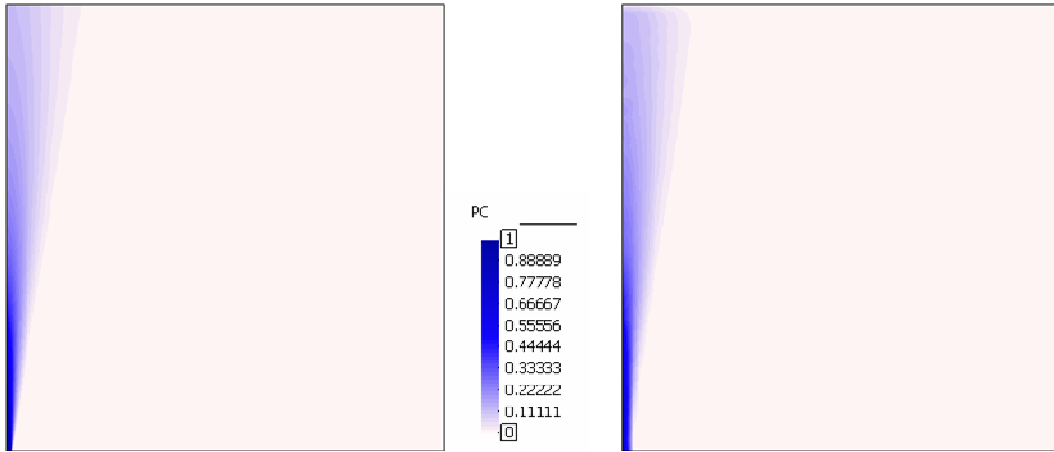Figure 7: Diagram of the axisymmetric free jet

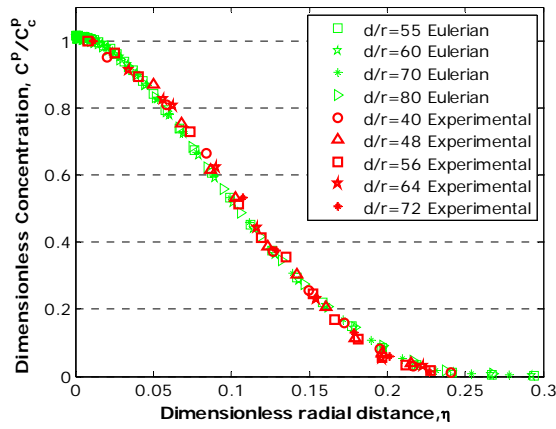Figure 8: Comparison of Eulerian (left) and Lagrangian (right) results

Figure 9: Experimental solution [32] (red) and Eulerian model results (green) for normalized self-preserving radial profiles of the concentration in free jet problem.
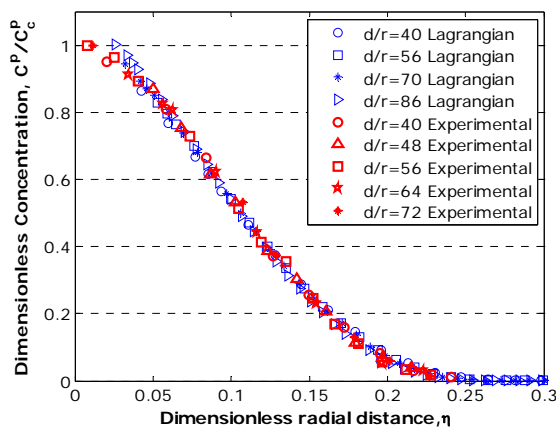

Figure 10: Experimental solution[32] (red) and Lagrangian model results (blue) for normalized self-preserving radial profiles of the concentration in free jet problem.